9

AUG 11 1998

ISAS-RN-656

Fermilab Library
0 1160 0067130 9

ISAS RESEARCH NOTE

ISAS RN 656

How Big Are Charge Clouds inside the Charge-Coupled Device Produced by X-Ray Photons ?

Junko Hiraga, Hiroshi Tsunemi, Kumi Yoshita,
Emi Miyata and Masayuki Ohtani

NAME | I.D. No

RETURN TO FERMILAB LIBRARY

THE INSTITUTE OF SPACE AND ASTRONAUTICAL SCIENCE

THE INSTITUTE OF SPACE AND ASTRONAUTICAL SCIENCE
YOSHINODAI, SAGAMIHARA, KANAGAWA 229-8510

ISAS RESEARCH NOTE

ISAS RN 656

How Big Are Charge Clouds inside the Charge-Coupled Device Produced by X-Ray Photons ?

Junko Hiraga[1,2], Hiroshi Tsunemi[1,2,3], Kumi Yoshita[1,2], Emi Miyata[1,2], and Masayuki Ohtani[1,2]

July 1998

[1] *Department of Earth and Space Science, Graduate School of Science, Osaka University*
1-1, Machikaneyama, Toyonaka, Osaka, 560-0043, Japan
[2] *CREST, Japan Science and Technology Corporation (JST)*
[3] *Institute of Space and Astronautical Science, 3-1-1 Yoshinodai, Sagamihara, Kanagawa 229-8510, Japan*

To appear in Jpn. J. Appl. Phys., vol. 37, No.8
URL: http://jjap.kopas.co.jp/journal/

How Big Are Charge Clouds inside the Charge-Coupled Device Produced by X-Ray Photons ?

*Junko HIRAGA [1,2], Hiroshi TSUNEMI [1,2], Kumi YOSHITA [1,2], Emi MIYATA [1,2] and Masayuki OHTANI [1,2]
[1]Department of Earth and Space Science,Graduate School of Science, Osaka University,
1-1 Machikaneyama-cho, Toyonaka, Osaka 560-0043, Japan
[2]CREST, Japan Science and Technology Corporation (JST)

To appear in Jpn. J. Appl. Phys. **37** (1998) No.8
URL: http://jjap.kopas.co.jp/journal/

ABSTRACT

We report here the charge cloud shape produced by an X-ray photon inside the CCD as well as a method to measure it. The measurement is carried out by using a multi-pitch mesh which enables us to specify the interaction position of X-rays with subpixel resolution not only for single events but also for split events. Split events are generated when the X-ray interaction position is close to the pixel boundary. The width of this area depends on the apparent charge size. Finally, we measured the signal output from the pixel according to the interaction position of X-rays. By differentiating this function, we obtain, in detail, the charge cloud shape which can be well represented by an asymmetric Gaussian function. The charge cloud size for Al-K X-rays is $0.7 \times 1.4\,\mu m^2$ while that for Mo-L X-rays is $0.8 \times 1.4\,\mu m^2$. The size of the photoelectron in Si produced by these X-rays is about $0.04\,\mu m$. Taking into account the mean absorption length for these X-rays in Si, diffusion process in the depletion region cannot explain the charge cloud size. The asymmetry of the charge cloud probably arises from the asymmetry of the electric field in the CCD.

KEY WORDS: charge-coupled-device, X-ray events, charge cloud shape, subpixel resolution

1. Introduction

Recently, a charge-coupled device (CCD) has been widely used for detection not only in the optical region but also in the X-ray region. The direct X-ray photon detection technique is now widely used in astronomy.[1, 2] The biggest difference between the X-ray photon and the optical photon is the number of electrons produced upon photoabsorption . The X-ray photon can produce a relatively large number of electrons upon photoabsorption while the optical photon can produce at the most one electron. After photoabsorption of the X-ray photon, the electron cloud diffuses to some extent before being collected below the gate of the CCD.[3] If the X-ray photon is photoabsorbed well inside the CCD pixel, the whole electron cloud is collected in one pixel forming a single event. If the X-ray photon is photoabsorbed near the pixel boundary, the electron cloud is split among 2–4 pixels depending on the interaction position of the X-ray photon, it forms a split event in which the sum of the split charge corresponds to the incident X-ray energy.

Since the CCD can produce signals only from each pixel, we cannot distinguish whether the charge produced by one X-ray photon splits into adjacent pixels or whether two or more X-ray photons enter the adjacent pixels. Therefore, we usually reduce the X-ray intensity so that two or more X-ray photons do not statistically enter the same or adjacent pixels in one exposure time. When we find adjacent pixels having signals under this condition, we conclude that

they are the split event produced by one X-ray photon.

A new technique has recently been introduced to identify the interaction position of the X-ray inside the pixel.[4] This technique enables us to experimentally determine that the X-rays form single events when they enter well within the pixel boundary and split events when they enter near the pixel boundary.[5, 6] There are two types of experiments[7]: a single-pitch mesh experiment and a multi-pitch mesh experiment. The single-pitch mesh experiment employs a mesh having small holes with spacing equal to the CCD pixel size. It produces a moire pattern which directly represents the pixel structure. However, it cannot always determine the hole position through which the X-ray enters. The multi-pitch mesh experiment employs a mesh having small holes with spacing equal to a multiple of the CCD pixel size. Although the moire pattern produced in this experiment does not directly show the pixel structure, we can uniquely determine the hole position through which the X-ray passes. Furthermore, the multi-pitch mesh experiment enables us to measure the charge cloud shape generated by X-ray photons.[8] This paper describes the comparison of the charge cloud shapes with different X-ray energies by this technique.

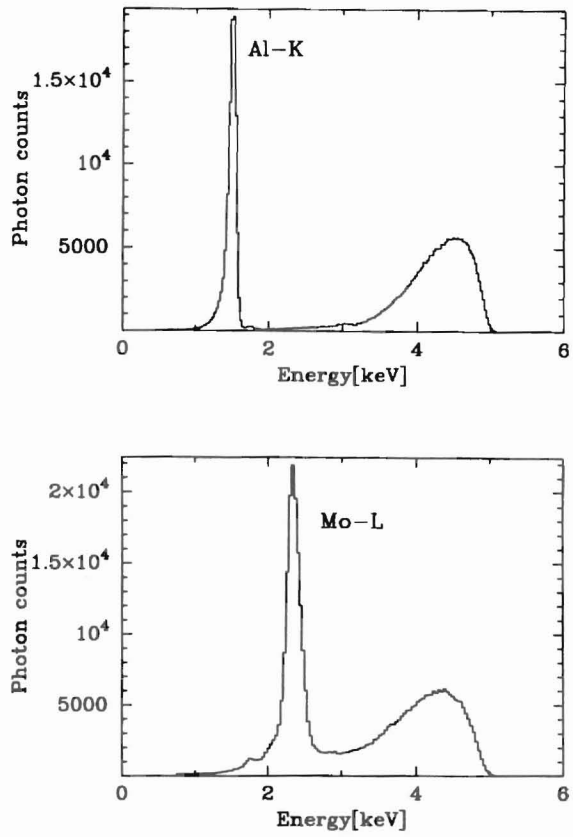

Fig. 1. The X-ray spectra obtained with the CCD in the mesh experiment for Al-K X-rays and Mo-L X-rays. The continuum above 3 keV is derived from the X-rays penetrating the copper foil while the characteristic X-rays are those passing through the hole. The Al-K X-rays consist of a single emission line while the Mo-L X-rays consist of two emission lines separated by 100 eV.

2. Experimental Setup

The basic idea of the mesh experiment has been described by Tsunemi et al.[4] It consists of a parallel X-ray beam and a metal mesh placed above a CCD. We employed a copper metal mesh with $10\,\mu m$ thickness having holes of $3.4\,\mu m$ diameter spaced at $48\,\mu m$. We used a CCD chip, N11-5-5A0N-2, (Hamamatsu Photonics) with $12\,\mu m^2$ pixel size. Hence, we performed a multi-pitch mesh experiment[7]: the hole spacing is a multiple of the CCD pixel spacing. The X-ray generator, the UltraX-18 (RIGAKU), employed two types of targets to generate characteristic X-rays with different energies. One is the Al-K X-ray (1.5 keV, the mean absorption length in Si is $7.9\,\mu m$) and the other is the Mo-L X-ray (2.2 keV, the mean absorption length in Si is $2.2\,\mu m$). The voltage applied to the X-ray generator was about 5 kV. The X-ray intensity was controlled such that the pile up did not cause a serious problem. Figure 1 shows the obtained X-ray spectra. The Al-K X-ray can be considered to be a single emission line while the Mo-L X-ray mainly consists of two emission lines separated by 100 eV. This is the cause of the apparent difference in line width between them.

The transmission of copper foil of $10\,\mu m$ thickness is 10^{-5} at the energy of Mo-L X-rays and lower at the energy of Al-K X-rays. Therefore, we can say that the X-ray continuum above 3 keV penetrates the copper foil while all the Al-K X-rays and Mo-L X-rays reach the CCD

through the mesh hole. We can select the X-ray events passing through the mesh hole by selecting the X-ray energy.

The CCD chip was cooled to $-60°C$. The CCD camera system was equipped with a mechanical shutter (stainless steel of $60\,\mu m$ thickness) to block X-rays during the readout time. Our system can obtain images every 30 s (including the data transfer time to a hard disk of a computer) selecting the exposure time of 5–10 s to maximize the number of isolated X-ray photons detected by the CCD. In this way, we operated the system for about 20 h, obtaining more than 1×10^5 single events for each X-ray.

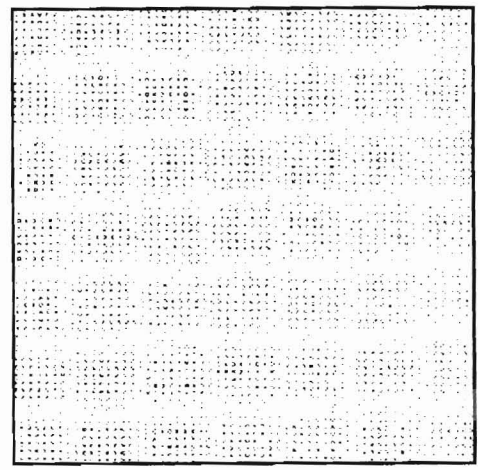

Fig. 2. A part of the raw image (250×250 pixels) obtained using single events is shown for Mo-L X-rays. Due to the multi-pitch mesh, most of the X-rays appear at roughly every 4×4 pixels.

3. Data Restoration Method

Figure 2 shows an example of the distribution of single events of X-rays obtained by our experiment. A clear moire pattern can be seen on the data. The detailed restoration method for the multi-pitch mesh experiment is described in Tsunemi et al.[7]

By using the restoration method, we obtain the exact relation between the CCD pixel coordinate and the mesh hole coordinate such that we can precisely determine the mesh hole corresponding to each CCD pixel. In this way, once we obtain the signal from a pixel, we can unequivocally determine the interaction position of the X-ray photon with subpixel resolution.

Figure 3 shows the representative pixel (RP) images of single events for Al-K X-rays and Mo-L X-rays. In these figures, we showed 3×3 RPs are shown. The pixel boundaries appear as bright regions in Fig. 3 where the X-rays form split events rather than single events. When an X-ray enters the boundary region of two pixels, 2-pixel split events are formed. When an X-ray enters the corner area of a pixel, the charge cloud is usually split among 3–4 pixels.[8]

4. Charge Cloud Shape

4.1. The amount of charge collected in one pixel

We employed the multi-pitch mesh in order to uniquely identify the interaction position of each event. We divided the RP into 20×20 subpixels. Then, we calculated all the X-ray events belonging to each subpixel. We found that there were $300 \sim 400$ X-ray events in each subpixel. In this way, we obtained the averaged event pattern for X-rays entering each subpixel.[8]

When the X-ray enters the CCD at the position of (X_p, Y_p), the output of the nth pixel of the CCD, $P_n(X_p, Y_p)$, is expressed by eq.(1).

$$P_n(X_p, Y_p) = \int_{X_n}^{X_{n+1}} dX \int_{Y_n}^{Y_{n+1}} dY\, f(X - X_p, Y - Y_p) \quad (1)$$

where $f(X, Y)$ describes the charge cloud shape just before the collection by the potential well. In our experimental setup, the actual output of the nth pixel, $D_n(X_{in}, Y_{in})$, is the convolution between $P_n(X_p, Y_p)$ and the mesh hole, which is given by eq.(2).

$$\begin{aligned} D_n(X_{in}, Y_{in}) &= \int dX_p \int dY_p P_n(X_p, Y_p) H(X_{in} - X_p, Y_{in} - Y_p) \\ &= \int_{X_n}^{X_{n+1}} dX \int_{Y_n}^{Y_{n+1}} dY\, f \otimes H(X - X_{in}, Y - Y_{in}) \quad (2) \end{aligned}$$

where $H(X, Y)$ shows a typical hole shape of the mesh and $f \otimes H$ represents the convolution between f and H.

$D_n(X_{in}, Y_{in})$ represents the average of the output from the nth pixel when the X-ray enters through the mesh hole in (X_{in}, Y_{in}). We can experimentally measure $D_n(X_{in}, Y_{in})$ by using the

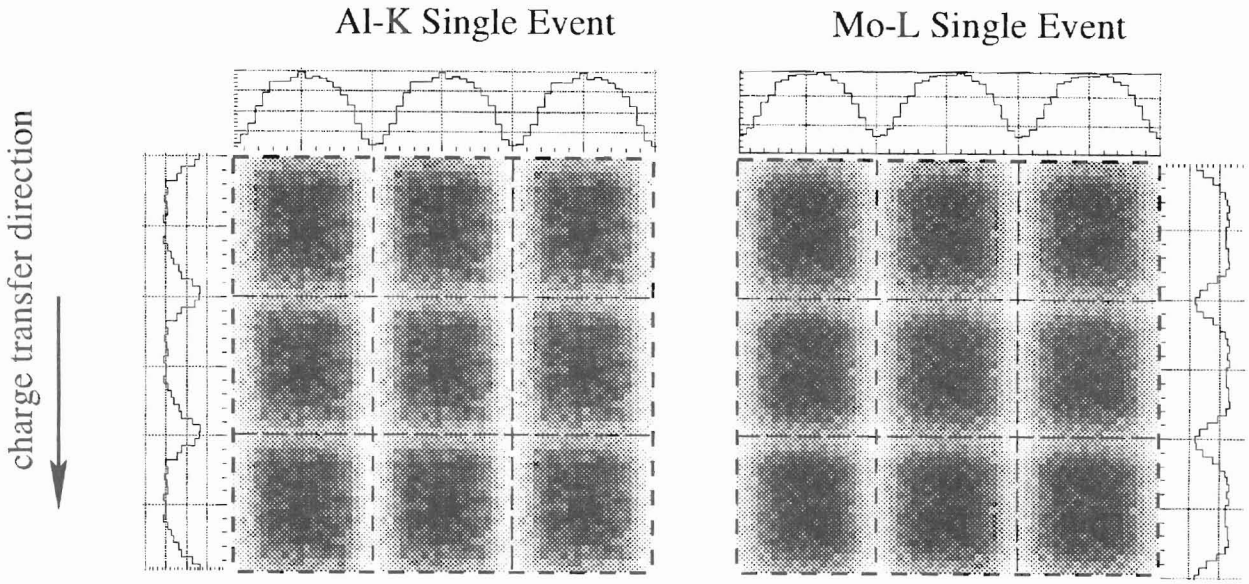

Fig. 3. The X-ray intensity map for single events of Al-K X-rays and of Mo-L X-rays with subpixel resolution. 3×3 RPs are shown. The pixel boundaries at every 12 μm are shown by dashed lines.

RP generated with all the X-ray events: both the single events and the split events. Figure 4 shows $D_n(X_{in}, Y_{in})$ for a 3×3 pixel region where the central pixel denotes the nth pixel. When the mesh hole is well within the nth pixel, the X-ray passing through the mesh hole forms a single event, consequently, the output of the nth pixel shows the X-ray energy. Therefore, a flat top is seen in the inner part of the central pixel of Fig. 4 where the X-ray becomes a single event.

When the mesh hole is near the pixel boundary, the X-ray passing through the mesh hole forms a split event. The output of the nth pixel reduces while the rest of the charge splits into adjacent pixels. When the mesh hole is on the pixel boundary, the output of the nth pixel represents approximately half the input X-ray energy. The output of the nth pixel reduces further as the mesh hole moves away from the nth pixel. Finally, no output is obtained when the mesh hole is away from the pixel boundary so that a single event is generated in the adjacent pixel. It should be noted that Fig. 4 is not related to the split threshold which determines whether the X-ray event becomes a single event or a split event.

4.2. Measuring the charge cloud shape

Next, we obtain the following relation by differentiating $D_n(X_{in}, Y_{in})$ with X_{in}, Y_{in}.

$$\begin{aligned}
&\frac{\partial^2}{\partial X_{in} \partial Y_{in}} D_n(X_{in}, Y_{in}) \\
&= \int_{Y_n}^{Y_{n+1}} \int_{X_n}^{X_{n+1}} f \otimes H_{XY}(X - X_{in}, Y - Y_{in}) dX dY \\
&= f \otimes H(X_{n+1} - X_{in}, Y_{n+1} - Y_{in}) \\
&\quad + f \otimes H(X_n - X_{in}, Y_n - Y_{in}) \\
&\quad - f \otimes H(X_{n+1} - X_{in}, Y_n - Y_{in}) \\
&\quad - f \otimes H(X_n - X_{in}, Y_{n+1} - Y_{in}) \qquad (3)
\end{aligned}$$

In this way, we will obtain $f \otimes H$ by differentiating the image in Fig. 4. In the practical calculation, the differential equation is replaced with the difference equation. When we differentiate D_n, four extremes at the pixel corners are obtained: two are positive and the other two are negative, as described in eq.(3) and as shown in Fig. 5.

Since these extremes are clearly separated from each other in our data, we combined four extremes to improve the statistics of the data. Figure 6 shows $f \otimes H$ which is the convolution between the charge cloud shape and the mesh hole shape. The obtained shapes can be well represented by Gaussian function whereas they

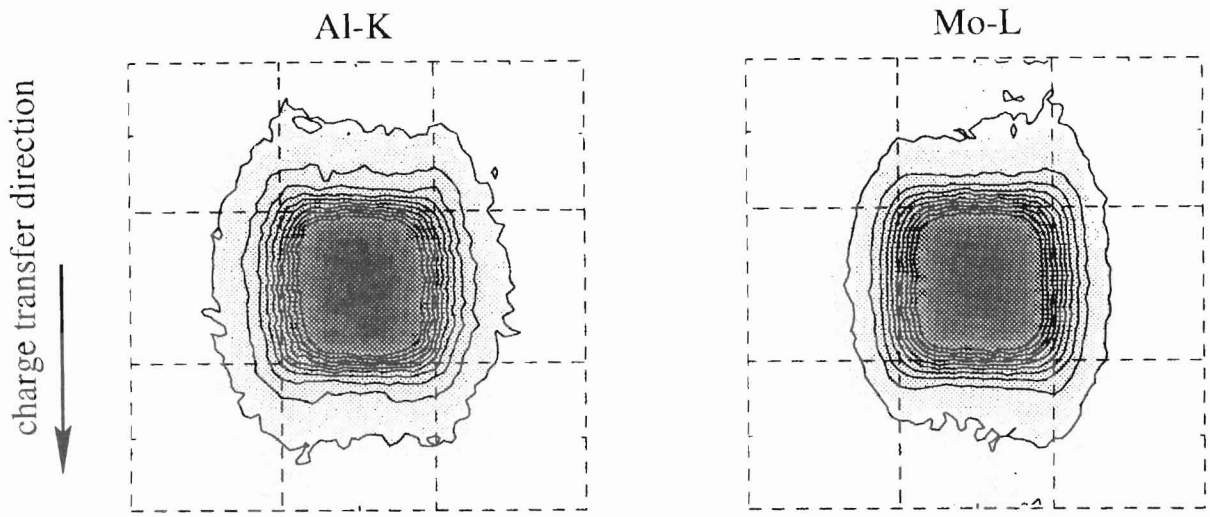

Fig. 4. The charge collected in the nth pixel is shown on the X-ray interaction position for Al-K X-rays and for Mo-L X-rays. The nth pixel and its 8 surrounding pixels are shown. The contours of the linear scale are overlaid.

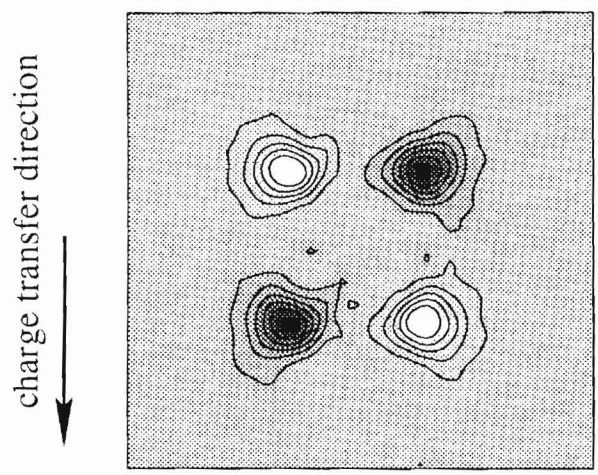

Fig. 5. Partial differentiate of D_n for Mo-L X-rays in Fig.4 is shown. There are four extremes at the RP corner: two are positive and the other two are negative as shown in eq.(3). The image shown here is smoothed by a Gaussian function of the width $\sigma = 1\,\mu m$.

show not point symmetry but axial symmetry. The effective hole diameter is $3.9\,\mu m$, taking into account the diffraction. We can deduce the size of the charge cloud shape and the results are summarized in Table 1.

4.3. Expansion of the charge cloud shape

As shown in Fig. 3, the width of the boundary region for Al-K X-rays looks similar to that for Mo-L X-rays. Since the width of the boundary region indicates the charge cloud size, [5] we expect the charge cloud size to be similar in both cases. In our experiment, it was determined by

Table 1. Charge cloud size produced by X-ray photons

	Al-K	Mo-L
Energy (keV)	1.5	2.2
Mean absorption length (μm)	7.9	2.2
Data width (X) (μm)	1.7 ±0.1	1.7 ±0.1
(Y) (μm)	1.2 ±0.1	1.3 ±0.1
Intrinsic width (X) (μm)	1.4 ±0.2	1.4 ±0.2
(Y) (μm)	0.7 ±0.2	0.8 ±0.2

three factors: the effective mesh hole size, the primary charge cloud size and the diffusion during the charge transfer to the potential well. The effective mesh hole size contributes to the charge cloud size by $0.95\,\mu m$ (standard deviation). The primary charge cloud size is expected to be less than $0.04\,\mu m$ [3] for the X-rays used.

The effect of diffusion depends on the interaction position of the X-ray. The CCD we used is assumed to have a depletion region of $6\,\mu m$ [9]. Taking into account the mean absorption length of X-rays, the Al-K X-rays are absorbed not only in the depletion region but also in the neutral region below it. If the X-rays are photoabsorbed below the depletion region, charge moving towards the gates will spread widely and form multi-pixel events. Furthermore, other charge moving away from the gates is lost in the substrate of the CCD. Those events are excluded in

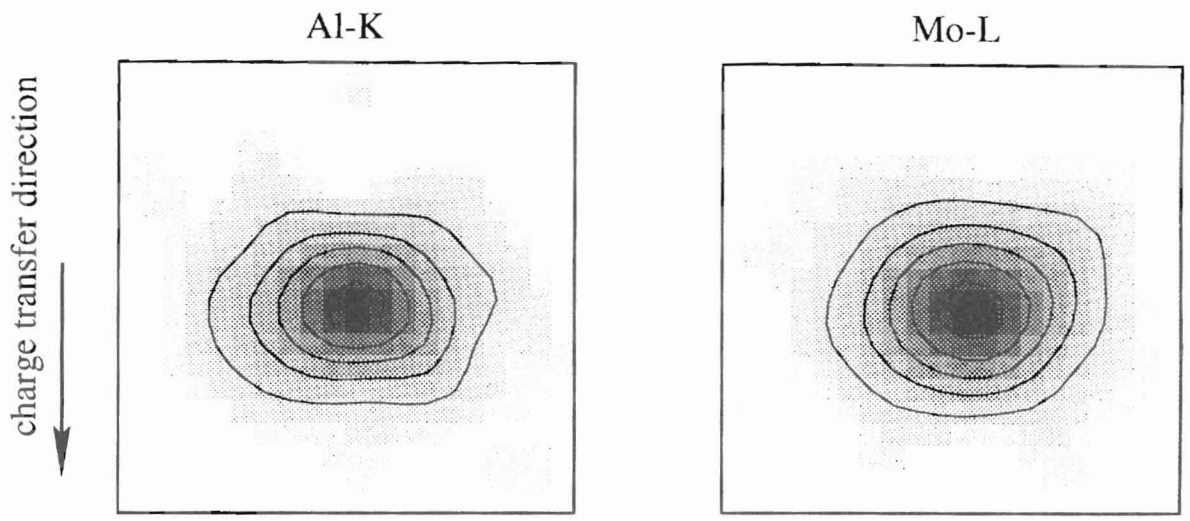

Fig. 6. Charge cloud shapes for Al-K X-rays and for Mo-L X-rays are shown in a pixel of $12\,\mu m^2$. Linear contour levels are overlaid. Gate structures run along the horizontal direction while the channel stop runs perpendicular to them. The image shown here is smoothed by a Gaussian function of the width $\sigma = 1\,\mu m$.

our analysis either by the selection of energy or by the number of split pixels. Therefore, the interaction depth of the Al-K X-rays scatter only inside the depletion region in our case. In contrast, the Mo-L X-rays would be photoabsorbed in a relatively shallow region of the depletion region due to the relatively short mean absorption length in Si. We found that the expected absorption depth in our experimental setup is $2.6\,\mu m$ for Al-K X-rays and $1.8\,\mu m$ for Mo-L X-rays, respectively.

The diffusion inside the depletion region can be estimated based on the numerical calculation. [3] The expected diffusion length is less than $0.1\,\mu m$ for the expected absorption depth in our experiment, which is consistent with our result revealing no significant difference between the charge cloud size for Al-K X-rays and that for Mo-L X-rays.

Yoshita *et al.* [5] estimated the charge cloud size from the width of the pixel boundary. They found that the charge cloud size depended weakly on the mean absorption length inside Si, which is consistent with our results. However, this is the first study to report charge cloud asymmetry. The width of the pixel boundary is strongly affected both by the complicated gate structure and the split threshold, whereas, the measured D_n is unrelated to ether, which yields a charge cloud shape free from a artificial parameters. Furthermore, we do not assume the cloud shape at all. Our method can uniquely determine the cloud shape if it is smaller than the mesh hole interval.

The charge cloud sizes we obtained are bigger than those expected from the numerical calculation. [3] Furthermore, they are asymmetric along the horizontal direction. Since the X-rays we used are unpolarized, the mean shape of the primary charge cloud is expected to be point-symmetric. The diffusion process does not produce a symmetric shape. Therefore, the asymmetric shape of the charge cloud be due to the characteristics of the CCD chip.

The electric field in the CCD pixel is generated both by the gate structure and the channel stop structure. The gate structure generates a potential well along the vertical direction while the channel stop structure generates one along the horizontal direction. Since these two structures are not identical to each other, the diffusion process in the vertical direction will be different from that in the horizontal direction, which could be the cause of the asymmetry of the primary charge clouds shown in Fig. 6.

Finally, we should note that the accuracy of the charge cloud shape measurement depends not on the CCD pixel size but on the mesh hole

size. If the CCD pixel size is big, the number of single events would increase and that of split events would decrease. Since the charge cloud shape is mainly determined not by single events but by split events, a large pixel size will reduce not the accuracy of the measurement but the efficiency of the measurement. If the CCD pixel size is sufficiently small, D_n itself would represent the charge cloud shape. Therefore, we can measure the charge cloud size using D_n.

5. Conclusion

We present here the results of a multi-pitch mesh experiment for X-rays with different energies. This technique unequivocally determines the X-ray interaction position inside the CCD pixel. The data are restored to obtain representative pixels (RP) showing the interaction region of X-rays where a single event or a split event is formed.

The output of the nth pixel, D_n, is obtained according to the interaction position of X-rays. This can be obtained not by the single-pitch mesh experiment but by the multi-pitch mesh experiment. By differentiating D_n, we calculated the charge cloud shape, $f(X, Y)$, taking into account the mesh hole size. The charge cloud shape for Al-K X-rays is similar to that for Mo-L X-rays, both being asymmetric. There are three factors determining the charge cloud size. [3] In our results the charge cloud sizes are bigger than those expected from numerical calculation. [3] Furthermore, they show asymmetric structure. The asymmetry of the charge cloud shapes we have shown probably arises from the difference in this study between the electric field along the gate structure and that along the channel stop structure. The accuracy of the charge cloud shape depends not on the CCD pixel size but on the mesh hole size.

6. Acknowledgements

The authors express their special thanks to Mr. K. Miyaguchi who technically supported this study.

Bibliography

[1] G. W. Frazer: *X-ray Detectors in Astronomy* (Cambridge University press, Cambridge, 1989) p. 208.

[2] Y. Tanaka, H. Inoue and S. S. Holt: Publ. Astron. Soc. Jpn. **46** (1994) 37.

[3] J. Janesick, T. Elliott and G. Garmire: Proc. SPIE **597** (1985) 364.

[4] H. Tsunemi, K. Yoshita, and S. Kitamoto: J.J. Appl. Phys. **36** (1997) 2906.

[5] K. Yoshita, H. Tsunemi, K. C. Gendreau, G. Pennington and M. W. Bautz: to be published in IEEE Trans. Nucl. Sci. **45** (1998).

[6] M. J. Pivovaroff, S. Jones, M. W. Bautz, S. Kissel, G. Prigozhin, G. R. Ricker, H. Tsunemi and E. Miyata: IEEE Trans. Nucl. Sci. **45** (1998) 164.

[7] H. Tsunemi, J. Hiraga, K. Yoshita, and S. Kitamoto: to be published in J.J. Appl. Phys. **37** (1998).

[8] H. Tsunemi, J. Hiraga, K. Yoshita and K. Hayashida: submitted to Nucl. Instr. and & Methods.

[9] K. Miyaguchi: private communication.